This is the accepted manuscript made available via CHORUS. The article has been published as:

Spin dependence of black hole ringdown nonlinearities

Jaime Redondo-Yuste, Gregorio Carullo, Justin L. Ripley, Emanuele Berti, and Vitor Cardoso

Phys. Rev. D **109**, L101503 — Published 21 May 2024

DOI: 10.1103/PhysRevD.109.L101503

Spin dependence of black hole ringdown nonlinearities

Jaime Redondo–Yuste,[1,*] Gregorio Carullo,[1] Justin L. Ripley,[2] Emanuele Berti,[3] and Vitor Cardoso[1,4]

[1] *Niels Bohr International Academy, Niels Bohr Institute, Blegdamsvej 17, 2100 Copenhagen, Denmark*
[2] *Illinois Center for Advanced Studies of the Universe & Department of Physics, University of Illinois at Urbana-Champaign, Urbana, Illinois 61801, USA*
[3] *William H. Miller III Department of Physics and Astronomy, Johns Hopkins University, 3400 North Charles Street, Baltimore, Maryland, 21218, USA*
[4] *CENTRA, Departamento de Física, Instituto Superior Técnico – IST, Universidade de Lisboa – UL, Avenida Rovisco Pais 1, 1049-001 Lisboa, Portugal*

The nonlinear character of general relativity leaves its imprint in the coalescence of two black holes, from the inspiral to the final ringdown stage. To quantify the impact of nonlinearities, we work at second order in black hole perturbation theory and we study the excitation of second-order modes relative to the first-order modes that drive them as we vary the black hole spin and the initial data for the perturbations. The relative amplitude of second-order modes is only mildly dependent on the initial data that we consider, but it strongly decreases for large black hole spins. This implies that the extrapolation of calculations based on the Kerr-CFT correspondence to subextremal Kerr black holes should be viewed with caution.

Introduction. The study of strong gravitational fields may unlock some of the most persistent puzzles in our understanding of fundamental interactions. The detection of gravitational waves from the merger of compact objects [1–4] turned strong gravity into an active and data-driven research field, allowing for new tests of general relativity (GR) in the nonlinear regime and, in particular, of black hole (BH) physics [5–10].

An especially appealing dynamical setting concerns the late stages of the coalescence of compact binaries, when the final BH relaxes to a stationary Kerr state, "ringing down" in a set of characteristic quasinormal modes (QNM) [11–13]. The "black hole spectroscopy" program is concerned with the details of this process, and it requires precise theoretical predictions to be compared against data [14, 15]. The frequencies of the QNMs are a benchmark prediction of GR, and they have been used to carry out consistency tests with LIGO-Virgo-KAGRA data [7, 9, 10, 16–23].

Most prior work on ringdown was done within linear perturbation theory, which is valid when the backreaction of the perturbations on the spacetime is negligible. However, right after the merger of two BHs backreaction is significant, and nonlinear phenomena have been identified in several studies (see e.g. [24–30]). In order to achieve high-precision ringdown tests, it is critical to understand the transition between the nonlinear and the linear regime. One example of a nonlinear effect are quadratic quasinormal modes (QQNMs): loosely speaking, these are driven, quadratic (and therefore, nonlinear) combinations of QNMs. The presence of these driven modes is predicted by second-order perturbation theory [31–38], and they play an important role in gravitational waveforms emitted by binary BH mergers [26, 28, 29]. Including these effects may be crucial to model certain high angular ringdown modes [39].

* jaime.redondo.yuste@nbi.ku.dk

In a spherical decomposition of the gravitational waveform, QQNMs are generated from linear QNMs through the channel $(\ell m)\times(\ell' m') \to (LM)$, with standard angular selection rules such that $M = m + m'$. Recently, the amplitude of the $L = M = 4$ QQNM was measured by fitting binary BH merger simulations in numerical relativity, and compared with the squared amplitude of the *parent* mode $\ell = \ell' = m = m' = 2$ [28, 29]. Focusing on the fundamental ($n = 0$) QNM contribution, both references obtained a similar value for the ratio

$$\mathcal{R}_{220\times220} = \frac{A_{220\times220}}{A_{220}^2} \sim 0.15 - 0.2\,, \tag{1}$$

where $A_{\ell mn}$ denotes the amplitude of the mode with angular numbers ℓm and overtone index n in a spin-weighted spheroidal harmonics decomposition ("parent mode"), and $A_{220\times220}$ denotes the amplitude of the QQNM resulting from the nonlinear interaction of a pair of 220 modes ("child mode").

A similar ratio was recently borne out of calculations using the Kerr/CFT$_2$ correspondence [40] (see also Ref. [41]), which assumes near-extremal BHs [42]. This result raises an interesting question: *is the ratio* (1) *generically independent of the characteristics of the perturbed Kerr BH, including its spin and the initial conditions of the perturbations?* Here we show that it is not.

Set-up. We study the evolution of a perturbed BH with mass M and angular momentum $J = Ma$ up to second order , with line element

$$g_{ab} = \bar{g}_{ab} + \varepsilon h^{(1)}_{ab} + \varepsilon^2 h^{(2)}_{ab}\,, \tag{2}$$

where $\bar{g}_{ab}$ is the background Kerr metric, $h^{(n)}_{ab}$ is the n–th order perturbation, and ε a perturbative parameter. The vacuum Einstein equations reduce to one master Teukolsky equation at each perturbative order [36, 43, 44]. Up

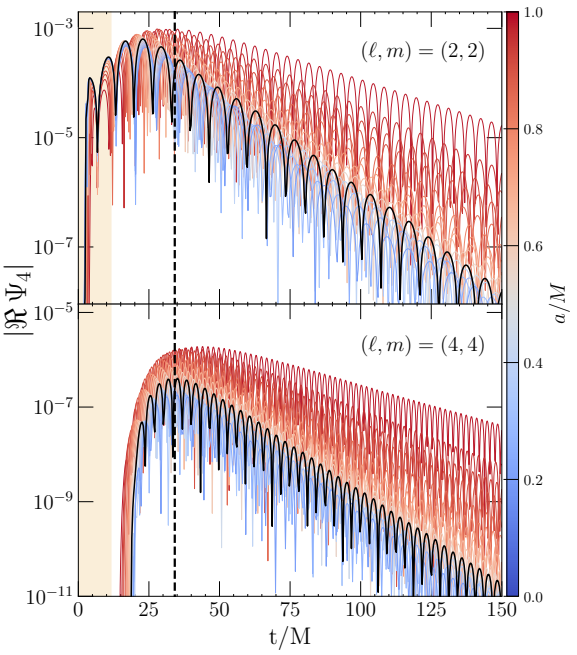


Figure 1. Absolute value of the real part of the perturbation scalar $\Psi_4^{(1/2)} = \mathcal{T}[h_{ab}^{(1/2)}]$ in the linear (top) and quadratic (bottom) sectors, for the angular modes indicated in the legend. Lines correspond to perturbations of a Kerr background with different spin a/M (different colors), excited by an initial profile with $\{A, r_l/r_h, r_u/r_h\} = \{0.01, 1.5, 2.5\}$, where $r_h \equiv M + \sqrt{M^2 - a^2}$. For the specific spin value $a/M = 0.5$ (black line) we show the reference timewhen the quadratic mode attains its maximum (vertical dashed line), and we also highlight in beige the region where constraint violations due to the initial data are present.

to second order, the system of equations is

$$\mathcal{O}_{-2}\mathcal{T}[h_{ab}^{(1)}] = 0\,, \quad \mathcal{O}_{-2}\mathcal{T}[h_{ab}^{(2)}] = \mathcal{S}[h_{cd}^{(1)}]\,, \tag{3}$$

where $\mathcal{O}_{-2}$ is the Teukolsky operator, and $\mathcal{T}$ is an operator that relates the metric perturbation to the Weyl scalar Ψ_4. The second-order equation is sourced by first-order fluctuations $\mathcal{S}[h_{cd}^{(1)}]$. We solve the Teukolsky equation $\mathcal{O}_{-2}\Psi_4^{(1)} = 0$ to obtain $\Psi_4^{(1)} = \mathcal{T}[h_{ab}^{(1)}]$, which at future null infinity can be directly related to the gravitational-wave strain by

$$\Psi_4 \xrightarrow{\mathscr{I}^+} -2\Big(\ddot{h}_+ - i\ddot{h}_\times\Big)\,, \tag{4}$$

where $h_{+,\times}$ are the two gravitational-wave polarizations (the prefactor of 2 is sensitive to the code's tetrad conventions [37, 45, 46]). Knowledge of the full $h_{ab}^{(1)}$ is not necessary to study gravitational radiation at first order, but it is required to build the source term to compute second-order quantities. The procedure to obtain $h_{ab}^{(1)}$ from $\Psi_4^{(1)}$ is known as metric reconstruction, and it is a topic of active research [36, 44, 47–49]. We reconstruct the metric $h_{ab}^{(1)}$ from $\Psi_4^{(1)}$ by directly integrating the Einstein equations in the Newman-Penrose formalism [36].

We numerically solve the system of equations (3) with the code described in Refs. [37, 45]. The code solves the Teukolsky equation and metric reconstruction equations on a horizon-penetrating, hyperboloidally compactified domain – i.e., it using coordinates stretching from the BH horizon to future null infinity on constant-time hypersurfaces. Initial data for $\Psi_4^{(1)}$ is given by:

$$\begin{aligned}\Psi_4^{(1)}(t=0) &= \phi_0\ {}_{-2}P_\ell^m(\vartheta)e^{im\phi}\,, \\ \phi_0 &= A\Big(\frac{r-r_l}{r_u-r_l}\Big)^2\Big(\frac{r_u-r}{r_u-r_l}\Big)^2 \\ &\quad\times \exp\Big(-\frac{1}{r-r_l} - \frac{2}{r_u-r}\Big)\theta(r-r_l)\theta(r_u-r)\,.\end{aligned} \tag{5}$$

Above, ${}_sP_\ell^m$ denotes the spin-weighted associated Legendre function, the numbers ℓ and m are constants which characterize the angular structure of the initial data, and θ denotes the Heaviside step function. The parameters $\{A, r_l, r_u\}$ characterize the initial profile, fixing respectively its amplitude, lower and upper radius. The initial velocity profile, $\partial_t\Psi_4^{(1)}$, is chosen so that the pulse moves towards the BH. We additionally set $h_{ab}^{(1)}\,(t=0) = 0$. While these initial data do not satisfy the Einstein constraint equations, so long as $|m| \geq 2$ the constraint violating modes propagate off of our computational domain in a finite amount of time T_R [37]. We set $\Psi_4^{(2)} = 0$, $h_{ab}^{(2)} = 0$, which satisfies the second-order Einstein constraint equations. Numerical convergence is discussed in the Supplemental Material (SM). As the numerical grid represents a hyperboloidal slicing of the Kerr background, we can extract $\Psi_4^{(1)}$ and $\Psi_4^{(2)}$ at null infinity. We then project those quantities onto spin-weighted spherical harmonics.

In Fig. 1 we show how the perturbations extracted at null infinity depend on the BH spin. The BH is initially perturbed by an incoming $\ell = m = 2$ mode (upper panel). The lower panel shows the $\ell = m = 4$ mode, excited due to the nonlinear contributions of the initial perturbation. Constraint violations have no significant impact on our ability to study second-order modes.

Ringdown model. To compare our results with Refs. [28, 29, 40], we study the strain amplitude h instead of Ψ_4. Our numerical simulations end before we observe a power-law tail, and the modeling starting time imposed by the metric reconstruction implies that the initial burst should not affect our calculations. Hence, for each of the spherical modes we consider a template consisting of a superposition of damped sinusoids

$$\begin{aligned}h_{\ell m}(t) = \sum_{\ell'=2}^{\infty}\sum_{n=0}^{\infty}\Big[&\mathcal{A}_{\ell' mn}\, e^{i(\omega_{\ell' mn}(t-t_0)+\phi_{\ell' mn})} \\ &+ \mathcal{A}_{\ell' -mn}\, e^{i(\omega_{\ell' -mn}(t-t_0)+\phi_{\ell' -mn})}\Big]\,,\end{aligned} \tag{6}$$

with $t > t_0$ and the complex frequencies $\omega_{\ell' mn}$ corre-

spond to the QNMs of a perturbed Kerr BH.[1] All amplitudes and phases will be defined with respect to the arbitrary reference time $t_0 = 0$, which we choose to coincide with the peak of the second-order perturbation (see Fig. 1). The sum on ℓ' is due to spherical-spheroidal mode mixing [50–54]. We compute the mixing coefficients using the Black Hole Perturbation Toolkit [55], as described in the SM. The first term corresponds to "corotating" (prograde) modes with $\mathrm{Re}\{\omega_{\ell mn}\} > 0$, while the second corresponds to "counterrotating" (retrograde) modes with $\mathrm{Re}\{\omega_{\ell -mn}\} < 0$, which are increasingly suppressed for large values of a/M [14, 56, 57]. As our model assumes a QNM-driven regime, we can analyze $\psi_{4,\ell m}$ and reconstruct the strain amplitudes by a simple frequency rescaling: $\mathcal{A}_{\ell mn} = (2\omega^2_{\ell mn})^{-1}\mathcal{A}^{\Psi}_{\ell mn}$, as dictated by Eq. (4) at future null infinity. This rescaling is in good agreement with an alternative calculation in which we compute the strain h through two direct integrations in time of Ψ_4, and then extract the amplitude of h, but it avoids the integrations (which increase numerical noise).

We refer to each of the two contributions to a given (ℓm) multipole of h as a "mode," each with an amplitude $\mathcal{A}_{\ell mn}$ and a phase $\phi_{\ell mn}$, treated as two unknown parameters to be inferred from the numerical data.

Bayesian mode extraction. We explored a wide range of initial conditions and spins. Properly accounting for errors on the fitting parameters is crucial, because some of the subdominant contributions can be comparable to the numerical resolution (this is true, e.g., for counterrotating modes and near-extremal spins). For this reason, we address the fitting problem through Bayesian inference [58]. In this way the numerical error is folded in the inferred parameters, yielding not only a point estimate of the quantities of interest, but the full information available at a given resolution (including the uncertainties).

The complex QNM frequencies are uniquely determined by the Kerr BH mass (which enters only as a scaling factor) and spin of each simulation. We choose uniform priors on all sampling parameters within the ranges $\ln \mathcal{A} \in [-15, 0]$ for the linear contributions, $\ln \mathcal{A} \in [-35, -5]$ for the quadratic contributions, and $\phi \in [0, 2\pi]$. The dominant uncertainty in the reconstruction is introduced by the resolution error, so we consider a gaussian likelihood, with an error at each time given by the difference between the two highest resolutions available. This choice guarantees a conservative and unbiased mode extraction, as we verified by simulating and recovering mock ringdown signals superimposed to the numerical error. To perform the extraction, we have developed a dedicated `python` package, `bayRing`, which we make publicly available [59]. The waveform model is interfaced through `pyRing` [17, 60], the QNM frequencies are computed through the `qnm` [61] package, and the high-dimensional parameter space exploration is achieved through the parallel nested sampling algorithm [62], as implemented in `raynest` [63]. We use 128 live points, and 256 maximum Markov Chain Monte Carlo (MCMC) steps. For each analysis, we run 4 parallel explorations, and combine them in a unique posterior distribution by weighting them through their Bayesian evidence. This last step is crucial to ensure that our estimate does not depend on the random initial seed (the most challenging fitting models contain up to 12 free parameters).

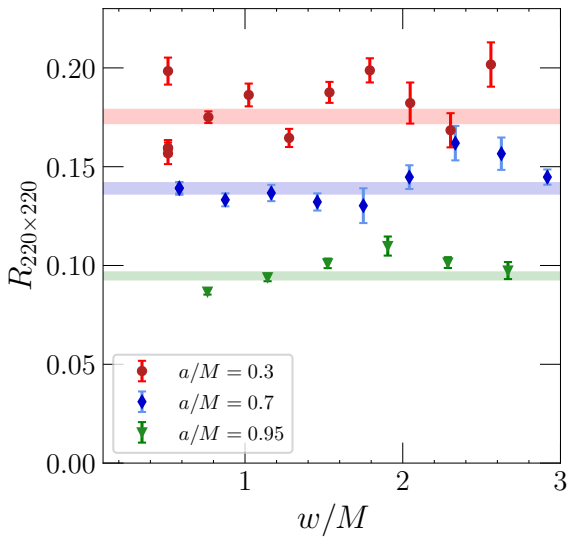


Figure 2. Ratio $\mathcal{R}_{220\times220} = A_{220\times220}/A^2_{220}$ as a function of the width of the initial pulse $w = r_u - r_l$, for a BH spin $a/M = [0.3, 0.7, 0.95]$ (in red, blue, green, respectively) and $r_l = 1.5 r_h$. Error bars indicate uncertainties due to numerical noise, the fitting procedure, mode selection, and the time shift problem. The average value (with its associated standard deviation) is shown as a colored shaded region. When a given value of w represents multiple points, those are computed using different values of r_l, further showing that the ratio depends only very mildly on the initial conditions.

In the SM we discuss how we take into account the starting time uncertainty (see [64, 65]) and possible additional systematic model uncertainties in our error budget, as well as the procedure used to select a "default set" of modes in our analysis. These modes are the $220, 2\text{-}20, 320, 221$ for the linear order, and the $440, 4\text{-}40$ and 220×220 for the second order perturbations.

Roughly speaking, our model and inference strategy are considered successful if the analysis residuals are smaller than the error induced by the numerics, and if we observe a saturation in the Bayesian evidence when including additional modes.

Dependence on the initial data. We have produced a catalog of runs with varying initial conditions and BH spins. For simplicity, we always consider initial condi-

[1] The frequencies correspond to a Kerr BH with mass and spin fixed by the initial conditions. Changes in the mass and spin are proportional to $(h^{(1)}_{ab})^2$, and thus, they do not affect the evolution of $\Psi^{(1)}$ and $\Psi^{(2)}$ to second order in perturbation theory. In general, higher-order perturbations (starting at cubic order, i.e., $\Psi^{(3)}$) would be sensitive to this effect [27].

tions in the spherical mode $(\ell, m) = (2, 2)$, so that the dominant quadratic mode is the 22×22. Our main results are summarized in Figs. 2 and 3.

An important question concerns the dependence of the nonlinear ratio $\mathcal{R}_{220\times220}$ on the initial data of Eq. (5). The overall amplitude A of the initial perturbation is a scaling factor, hence it must factor out of the ratio, but there could be nontrivial dependence of this ratio on other parameters, such as the location of the inner boundary, r_l, and the "width" of the initial pulse, $w = r_u - r_l$. In Fig. 2 we show that the ratio is only mildly dependent (if at all) on r_l and w. The figure shows that the mild dependence on initial conditions is valid for all values of the spins. Notice that for smaller spins, due to the increased relevance of counterrotating modes, the uncertainties in the extraction are larger.

The uncertainties in the extraction also become larger as the pulse becomes wider ($w \geq 3r_h$) or it is placed further away from the horizon ($r_l \geq 2r_h$). This is due to two reasons: the numerical evolution code uses hyperboloidal, compactified coordinates, and thus it needs more resolution to resolve features that are further away from the horizon or from null infinity. Moreover, initial pulses located far away correspond to a larger value of T_R, and this affects the time window of the signal available for the fit. The range of initial conditions we explored is not large enough to conclude that $\mathcal{R}_{220\times220}$ is constant across the whole parameter space.

The results reported in Fig. 2 can be recovered analytically, assuming that the system is in a QNM-driven regime. Take the first-order perturbation to be a single mode: $\Psi_4^{(1)} = A_{220} f(R) e^{i\omega_{220}(t-t_0)}$, with $f(R)$ a normalized eigenfunction ($f(R=0)=1$) in terms of the compactified coordinate where $R = 0$ corresponds to $\mathscr{I}^+$. Then, the initial conditions only affect the value of A_{220} [67, 68]. The inhomogeneous part of the second-order perturbation is given by $\Psi_4^{(2)}(t,R) = \int dR' G(R,R') \mathcal{S}[\Psi_4^{(1)}]$, where $G(R,R')$ is the radial Green's function associated to $\mathcal{O}_{-2}$, and $\mathcal{S}$ is the quadratic source term. Assuming a similar QNM structure for the quadratic perturbation (i.e., $\Psi_4^{(2)} = A_{220\times220} g(R) e^{2i\omega_{220}(t-t_0)}$, with $g(R=0)=1$) we have

$$\mathcal{R}_{220\times220} = \frac{A_{220\times220}}{A_{220}^2} = \int dR' G(0,R') \mathcal{S}[f(R')] \,, \quad (7)$$

where the quadratic source term depends only on the radial profile of the linear mode. This suggests that the ratio $\mathcal{R}_{220\times220}$ has no dependence on the initial conditions, as long as the nonlinear mode is generated exclusively via quadratic effects on a single mode. However, nonlocal behaviour of the source term may result in some nontrivial dependence on the initial conditions.

Dependence on BH spin. The dependence on the spin can be studied in a similar way. We now assume the pulse to be at $r_l = 1.5 r_h$, with width $w = r_h$. The Green's function and the source term depend explicitly on the BH spin, thus Eq. (7) suggests that the nonlinear ratio will have a nontrivial spin dependence.

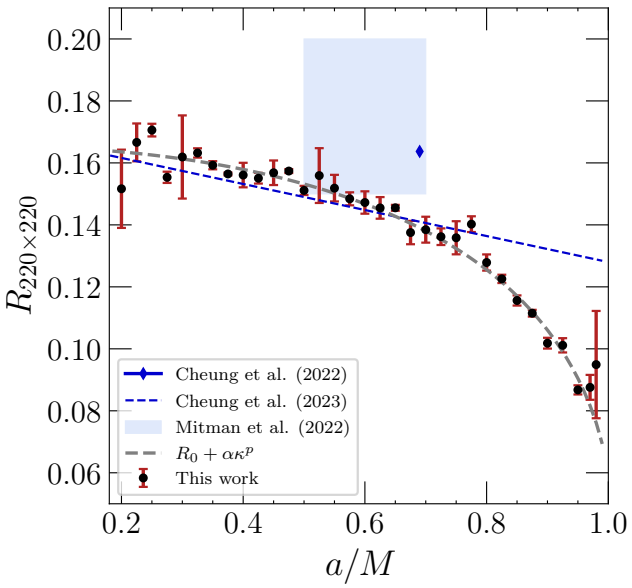


Figure 3. Ratio $\mathcal{R}_{220\times220}$, as a function of the spin of the remnant BH. The value decreases with the spin, especially as one approaches the extremal limit. The gray dashed line represents the best fit of the data points assuming a power law in terms of the surface gravity κ, $\mathcal{R}_{220\times220} = R_0 + (M\kappa)^p$. The best fit parameters are given in Eq. (8). We also represent the values for the non–linear ratio $\mathcal{R}_{220\times220}$ obtained originally from NR in [28] (referred to as Cheung et al.) and [29] (referred to as Mitman et al.). The blue dashed line corresponds to the linear hyperfit reported in [69], based on a catalogue of NR simulations.

Our results are summarized in Fig. 3: there is no universality, and the ratio $\mathcal{R}_{220\times220}$ is indeed spin-dependent and decreases with spin, ranging roughly between $\mathcal{R}_{220\times220} = 0.16$ for $a/M = 0.2$ and $\mathcal{R}_{220\times220} = 0.08$ for $a/M = 0.98$. These variations are much larger than the estimated uncertainties, or than possible variations due to the mild dependence on the initial conditions. The values that we extract, moreover, are surprisingly close to the resulting nonlinear ratio reported in [28, 29]. The spin-dependence of $\mathcal{R}_{220\times220}$ is well fitted by a power law of the surface gravity $\kappa = \frac{\sqrt{M^2-a^2}}{2M(M+\sqrt{M^2-a^2})}$: our results are well fitted to an expression of the form $\mathcal{R}_{220\times220} = R_0 + (M\kappa)^p$, with

$$R_0 = 0.058 \pm 0.003, \quad p = 1.61 \pm 0.03 \,. \quad (8)$$

Uncertainties in the ratio extraction become smaller for rapidly spinning BHs, since at low spins counterrotating modes are as important as corotating ones. As a consequence, especially for the quadratic modes, our template should be enhanced with all the counterrotating contributions [14, 56, 57, 69], including the highly damped overtone and mode-mixing ones [50–54], severely complicating the inference problem and increasing computational

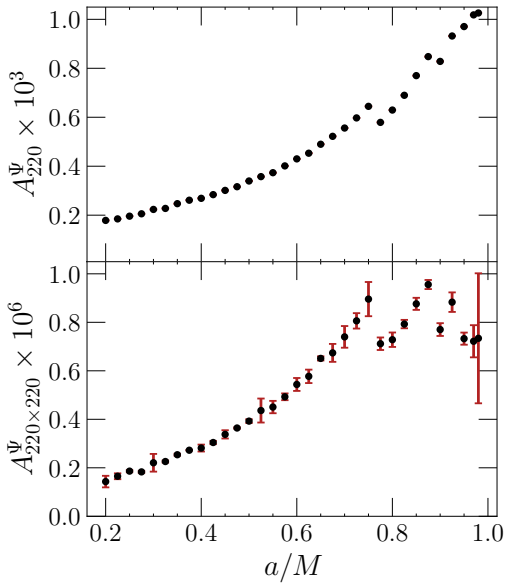


Figure 4. Amplitude of the fundamental 220 mode (top) and of the quadratic 220×220 mode (bottom) as a function of the BH spin. Notice that the amplitudes reported here refer to the master variable Ψ_4 and not to the GW strain.

cost. These contributions include, for example, mode-mixing terms such as the 640 mode or the 541 overtone, as well as additional quadratic terms such as $220 \times$ 2-20 mode. This is not of practical concern, since if universality does not happen already for this range of spins, there is no reason to expect universality to appear at lower spins. For this reason we do not include spins $a < 0.2$.

It is perhaps surprising that the nonlinear ratio $\mathcal{R}_{220\times220}$ decreases as the BH spin increases, but it does not imply that nonlinearities are becoming smaller. In Fig. 4 we show that both the amplitude $\mathcal{A}_{220}$ of the linear and $\mathcal{A}_{220\times220}$ of the nonlinear mode *grow* with BH spin, resulting in a ratio (1) which behaves as in Fig. 3. Since highly spinning BHs dissipate energy less efficiently, they could be more prone to nonlinearities. The ratio that we study quantifies the strength of a process which transfers energy from low- to higher energy scales. If nonlinear turbulent dynamics suppresses it, in a manner similar to fluids in two spatial dimensions [39, 70–73], perhaps explaining a lower $\mathcal{R}_{220\times220}$ at high spins.

Another feature apparent in Fig. 4 is a "kink" around $a/M \sim 0.75$. One possible explanation for this feature is the fact that on the equatorial plane ($\theta = \pi/2$), the light ring (which dominates QNM excitation) is inside the ergoregion exactly at $a/M = 1/\sqrt{2} \sim 0.7$. This could result in a qualitatively different behavior of the QNM excitation coefficients. Further clarification of this feature is left for future work.

Conclusions. The full nonlinear content of Einstein's equations is currently accessible only via simulations in numerical relativity. However, essential insight can be obtained with various degrees of approximation. The next step in a BH spectroscopy program requires the understanding of second-order effects. We uncovered essential aspects of such higher-order terms, including a mild dependence on initial conditions, and a strong dependence on the BH spin.

Remarkably, our results concerning the spin-dependence of the quadratic vs linear amplitudes ratio are in good agreement with the values reported from full nonlinear numerical simulations. Another recent study [74] explores the initial data and spin-dependence of the quadratic coefficient using both the second-order code employed here, and numerical relativity, albeit with a different mode inclusion criterion. Close agreement is observed between the two studies, together with similar consistency with nonlinear simulations (c.f. our Fig 3 with Fig.1 in [74]). Our results also show good agreement with semi–analytical calculations [75].

Finally, the amplitude of first-order terms observed in our detectors is $h^{(1)} \sim 10^{-21}$, and one might be tempted to infer that $h^{(2)} \sim (h^{(1)})^2 \sim 10^{-42}$. The correct scaling is instead $rh^{(2)} \sim (rh^{(1)})^2$ (one can see this directly in a gauge-invariant formalism, where second-order master wavefunctions $\Psi \propto rh$ are sourced by quadratic first-order terms [31–34]). Quadratic terms *are* important.

Acknowledgments. We thank Mark Ho-Yeuk Cheung, Alex Kehagias, Davide Perrone, and Toni Riotto for fruitful discussions. We are indebted to Hengrui Zhu for very useful discussions, and help in uncovering a data reading mistake in the initial version of this work. G.C. thanks William East, Luis Lehner, Taillte May and Huan Yang for stimulating discussions, and Perimeter Institute for the generous hospitality during the last stages of this work. J.L.R. thanks Hengrui Zhu for a helpful discussion on the tetrad normalization convention used in `SpEC`, and helpful conversations on nonlinear ringdown more generally. J.R-Y, G.C. and V.C. acknowledge support by VILLUM Foundation (grant no. VIL37766) and the DNRF Chair program (grant no. DNRF162) by the Danish National Research Foundation. G.C. also acknowledges funding from the European Union's Horizon 2020 research and innovation program under the Marie Sklodowska-Curie grant agreement No. 847523 'INTERACTIONS'. J.L.R. acknowledges support from the Simons Foundation through Award number 896696. E.B. is supported by NSF Grants No. AST-2006538, PHY-2207502, PHY-090003 and PHY-20043, by NASA Grants No. 20-LPS20-0011 and 21-ATP21-0010, by the John Templeton Foundation Grant 62840, by the Simons Foundation, by the Amaldi Research Center, and by the Italian Ministry of Foreign Affairs and International Cooperation Grant No. PGR01167. E.B. also acknowledges the support of the Indo-US Science and Technology Forum through the Indo-US Centre for Gravitational Physics and Astronomy, grant IUSSTF/JC-142/2019. V.C. is a Villum Investigator and a DNRF Chair. V.C. acknowledges financial support provided under the European Union's H2020 ERC Advanced Grant "Black holes: gravitational engines of discovery" grant agreement no.

Gravitas–101052587. Views and opinions expressed are however those of the author only and do not necessarily reflect those of the European Union or the European Research Council. Neither the European Union nor the granting authority can be held responsible for them. This project has received funding from the European Union's Horizon 2020 research and innovation programme under the Marie Sklodowska-Curie grant agreement No 101007855. This research was supported in part by Perimeter Institute for Theoretical Physics. Research at Perimeter Institute is supported in part by the Government of Canada through the Department of Innovation, Science and Economic Development Canada and by the Province of Ontario through the Ministry of Colleges and Universities.

[1] B. P. Abbott *et al.*, Observation of Gravitational Waves from a Binary Black Hole Merger, Phys. Rev. Lett. **116**, 061102 (2016).

[2] J. Aasi *et al.* (LIGO Scientific Collaboration), Advanced LIGO, Classical Quantum Gravity **32**, 074001 (2015), arXiv:1411.4547 [gr-qc].

[3] F. Acernese *et al.* (Virgo Collaboration), Advanced Virgo: a second-generation interferometric gravitational wave detector, Classical Quantum Gravity **32**, 024001 (2015), arXiv:1408.3978 [gr-qc].

[4] T. Akutsu *et al.* (KAGRA), Overview of KAGRA: Detector design and construction history, (2020), arXiv:2005.05574 [physics.ins-det].

[5] E. Berti *et al.*, Testing General Relativity with Present and Future Astrophysical Observations, Class. Quant. Grav. **32**, 243001 (2015), arXiv:1501.07274 [gr-qc].

[6] L. Barack *et al.*, Black holes, gravitational waves and fundamental physics: a roadmap, Class. Quant. Grav. **36**, 143001 (2019), arXiv:1806.05195 [gr-qc].

[7] B. P. Abbott *et al.* (LIGO Scientific, Virgo), Tests of general relativity with GW150914, Phys. Rev. Lett. **116**, 221101 (2016), [Erratum: Phys.Rev.Lett. 121, 129902 (2018)], arXiv:1602.03841 [gr-qc].

[8] B. P. Abbott *et al.* (LIGO Scientific, Virgo), Tests of General Relativity with the Binary Black Hole Signals from the LIGO-Virgo Catalog GWTC-1, Phys. Rev. D **100**, 104036 (2019), arXiv:1903.04467 [gr-qc].

[9] R. Abbott *et al.* (LIGO Scientific, Virgo), Tests of general relativity with binary black holes from the second LIGO-Virgo gravitational-wave transient catalog, Phys. Rev. D **103**, 122002 (2021), arXiv:2010.14529 [gr-qc].

[10] R. Abbott *et al.* (LIGO Scientific, VIRGO, KAGRA),

Tests of General Relativity with GWTC-3, (2021), arXiv:2112.06861 [gr-qc].
[11] K. D. Kokkotas and B. G. Schmidt, Quasinormal modes of stars and black holes, Living Rev. Rel. **2**, 2 (1999), arXiv:gr-qc/9909058.
[12] E. Berti, V. Cardoso, and A. O. Starinets, Quasinormal modes of black holes and black branes, Class. Quant. Grav. **26**, 163001 (2009), arXiv:0905.2975 [gr-qc].
[13] R. A. Konoplya and A. Zhidenko, Quasinormal modes of black holes: From astrophysics to string theory, Rev. Mod. Phys. **83**, 793 (2011), arXiv:1102.4014 [gr-qc].
[14] E. Berti, V. Cardoso, and C. M. Will, On gravitational-wave spectroscopy of massive black holes with the space interferometer LISA, Phys. Rev. D **73**, 064030 (2006), arXiv:gr-qc/0512160.
[15] E. Berti, A. Sesana, E. Barausse, V. Cardoso, and K. Belczynski, Spectroscopy of Kerr black holes with Earth- and space-based interferometers, Phys. Rev. Lett. **117**, 101102 (2016), arXiv:1605.09286 [gr-qc].
[16] R. Brito, A. Buonanno, and V. Raymond, Black-hole Spectroscopy by Making Full Use of Gravitational-Wave Modeling, Phys. Rev. D **98**, 084038 (2018), arXiv:1805.00293 [gr-qc].
[17] G. Carullo, W. Del Pozzo, and J. Veitch, Observational Black Hole Spectroscopy: A time-domain multimode analysis of GW150914, Phys. Rev. D **99**, 123029 (2019), [Erratum: Phys.Rev.D 100, 089903 (2019)], arXiv:1902.07527 [gr-qc].
[18] G. Carullo, Enhancing modified gravity detection from gravitational-wave observations using the parametrized ringdown spin expansion coeffcients formalism, Phys. Rev. D **103**, 124043 (2021), arXiv:2102.05939 [gr-qc].
[19] G. Carullo, D. Laghi, N. K. Johnson-McDaniel, W. Del Pozzo, O. J. C. Dias, M. Godazgar, and J. E. Santos, Constraints on Kerr-Newman black holes from merger-ringdown gravitational-wave observations, Phys. Rev. D **105**, 062009 (2022), arXiv:2109.13961 [gr-qc].
[20] R. Cotesta, G. Carullo, E. Berti, and V. Cardoso, Analysis of Ringdown Overtones in GW150914, Phys. Rev. Lett. **129**, 111102 (2022), arXiv:2201.00822 [gr-qc].
[21] H. O. Silva, A. Ghosh, and A. Buonanno, Black-hole ringdown as a probe of higher-curvature gravity theories, Phys. Rev. D **107**, 044030 (2023), arXiv:2205.05132 [gr-qc].
[22] E. Finch and C. J. Moore, Searching for a ringdown overtone in GW150914, Phys. Rev. D **106**, 043005 (2022), arXiv:2205.07809 [gr-qc].
[23] M. Crisostomi, K. Dey, E. Barausse, and R. Trotta, Neural Posterior Estimation with guaranteed exact coverage: the ringdown of GW150914, (2023), arXiv:2305.18528 [gr-qc].
[24] Y. Zlochower, R. Gomez, S. Husa, L. Lehner, and J. Winicour, Mode coupling in the nonlinear response of black holes, Phys. Rev. D **68**, 084014 (2003), arXiv:gr-qc/0306098.
[25] E. Abdalla, C. B. M. H. Chirenti, and A. Saa, Quasinormal modes for the Vaidya metric, Phys. Rev. D **74**, 084029 (2006), arXiv:gr-qc/0609036.
[26] L. London, D. Shoemaker, and J. Healy, Modeling ringdown: Beyond the fundamental quasinormal modes, Phys. Rev. D **90**, 124032 (2014), [Erratum: Phys.Rev.D 94, 069902 (2016)], arXiv:1404.3197 [gr-qc].
[27] L. Sberna, P. Bosch, W. E. East, S. R. Green, and L. Lehner, Nonlinear effects in the black hole ringdown: Absorption-induced mode excitation, Phys. Rev. D **105**, 064046 (2022).
[28] M. H.-Y. Cheung *et al.*, Nonlinear Effects in Black Hole Ringdown, Phys. Rev. Lett. **130**, 081401 (2023), arXiv:2208.07374 [gr-qc].
[29] K. Mitman *et al.*, Nonlinearities in Black Hole Ringdowns, Phys. Rev. Lett. **130**, 081402 (2023), arXiv:2208.07380 [gr-qc].
[30] V. Baibhav, M. H.-Y. Cheung, E. Berti, V. Cardoso, G. Carullo, R. Cotesta, W. Del Pozzo, and F. Duque, Agnostic black hole spectroscopy: quasinormal mode content of numerical relativity waveforms and limits of validity of linear perturbation theory, (2023), arXiv:2302.03050 [gr-qc].
[31] R. J. Gleiser, C. O. Nicasio, R. H. Price, and J. Pullin, Second order perturbations of a Schwarzschild black hole, Class. Quant. Grav. **13**, L117 (1996), arXiv:gr-qc/9510049.
[32] D. Brizuela, J. M. Martin-Garcia, and M. Tiglio, A Complete gauge-invariant formalism for arbitrary second-order perturbations of a Schwarzschild black hole, Phys. Rev. D **80**, 024021 (2009), arXiv:0903.1134 [gr-qc].
[33] K. Ioka and H. Nakano, Second and higher-order quasi-normal modes in binary black hole mergers, Phys. Rev. D **76**, 061503 (2007), arXiv:0704.3467 [astro-ph].
[34] H. Nakano and K. Ioka, Second Order Quasi-Normal Mode of the Schwarzschild Black Hole, Phys. Rev. D **76**, 084007 (2007), arXiv:0708.0450 [gr-qc].
[35] E. Pazos, D. Brizuela, J. M. Martin-Garcia, and M. Tiglio, Mode coupling of Schwarzschild perturbations: Ringdown frequencies, Phys. Rev. D **82**, 104028 (2010), arXiv:1009.4665 [gr-qc].
[36] N. Loutrel, J. L. Ripley, E. Giorgi, and F. Pretorius, Second Order Perturbations of Kerr Black Holes: Reconstruction of the Metric, Phys. Rev. D **103**, 104017 (2021), arXiv:2008.11770 [gr-qc].
[37] J. L. Ripley, N. Loutrel, E. Giorgi, and F. Pretorius, Numerical computation of second order vacuum perturbations of Kerr black holes, Phys. Rev. D **103**, 104018 (2021), arXiv:2010.00162 [gr-qc].
[38] M. Lagos and L. Hui, Generation and propagation of nonlinear quasinormal modes of a Schwarzschild black hole, Phys. Rev. D **107**, 044040 (2023), arXiv:2208.07379 [gr-qc].
[39] H. Yang, A. Zimmerman, and L. Lehner, Turbulent Black Holes, Phys. Rev. Lett. **114**, 081101 (2015).
[40] A. Kehagias, D. Perrone, A. Riotto, and F. Riva, Explaining nonlinearities in black hole ringdowns from symmetries, Phys. Rev. D **108**, L021501 (2023), arXiv:2301.09345 [gr-qc].
[41] T. Guerreiro, Nonlinearities in Black Hole Ringdowns and the Quantization of Gravity, (2023), arXiv:2306.09974 [gr-qc].
[42] M. Guica, T. Hartman, W. Song, and A. Strominger, The Kerr/CFT Correspondence, Phys. Rev. D **80**, 124008 (2009), arXiv:0809.4266 [hep-th].
[43] S. A. Teukolsky, Perturbations of a rotating black hole. 1. Fundamental equations for gravitational electromagnetic and neutrino field perturbations, Astrophys. J. **185**, 635 (1973).
[44] M. Campanelli and C. O. Lousto, Second order gauge invariant gravitational perturbations of a Kerr black hole, Phys. Rev. D **59**, 124022 (1999), arXiv:gr-qc/9811019.
[45] J. Ripley, JLRipley314/teuk-fortran-2020: Teuk-

Fortran-2020-v1.1 (2023).
[46] H. Zhu, A. Cardenas-Avendano, J. Ripley, and F. Pretorius, in. prep., .
[47] R. M. Wald, Construction of solutions of gravitational, electromagnetic, or other perturbation equations from solutions of decoupled equations, Physical Review Letters **41**, 203 (1978).
[48] S. R. Green, S. Hollands, and P. Zimmerman, Teukolsky formalism for nonlinear Kerr perturbations, Class. Quant. Grav. **37**, 075001 (2020), arXiv:1908.09095 [gr-qc].
[49] A. Spiers, A. Pound, and J. Moxon, Second-order Teukolsky formalism in Kerr spacetime: formulation and nonlinear source, (2023), arXiv:2305.19332 [gr-qc].
[50] E. Berti, V. Cardoso, and M. Casals, Eigenvalues and eigenfunctions of spin-weighted spheroidal harmonics in four and higher dimensions, Phys. Rev. D **73**, 024013 (2006), [Erratum: Phys.Rev.D 73, 109902 (2006)], arXiv:gr-qc/0511111.
[51] A. Buonanno, G. B. Cook, and F. Pretorius, Inspiral, merger and ring-down of equal-mass black-hole binaries, Phys. Rev. D **75**, 124018 (2007), arXiv:gr-qc/0610122.
[52] B. J. Kelly and J. G. Baker, Decoding mode mixing in black-hole merger ringdown, Phys. Rev. D **87**, 084004 (2013), arXiv:1212.5553 [gr-qc].
[53] E. Berti and A. Klein, Mixing of spherical and spheroidal modes in perturbed Kerr black holes, Phys. Rev. D **90**, 064012 (2014), arXiv:1408.1860 [gr-qc].
[54] L. London and E. Fauchon-Jones, On modeling for Kerr black holes: Basis learning, QNM frequencies, and spherical-spheroidal mixing coefficients, Class. Quant. Grav. **36**, 235015 (2019), arXiv:1810.03550 [gr-qc].
[55] Black Hole Perturbation Toolkit, (bhptoolkit.org).
[56] H. Lim, G. Khanna, A. Apte, and S. A. Hughes, Exciting black hole modes via misaligned coalescences: II. The mode content of late-time coalescence waveforms, Phys. Rev. D **100**, 084032 (2019), arXiv:1901.05902 [gr-qc].
[57] X. Li, L. Sun, R. K. L. Lo, E. Payne, and Y. Chen, Angular emission patterns of remnant black holes, Phys. Rev. D **105**, 024016 (2022), arXiv:2110.03116 [gr-qc].
[58] E. T. Jaynes, *Probability Theory: The Logic of Science* (Cambridge University Press, Cambridge, UK, 2003).
[59] G. Carullo, M. De Amicis, and J. Redondo-Yuste, bayring, github.com/GCArullo/bayRing (2023).
[60] G. Carullo, W. Del Pozzo, and J. Veitch, `pyRing`: a time-domain ringdown analysis python package, git.ligo.org/lscsoft/pyring (2023).
[61] L. C. Stein, qnm: A Python package for calculating Kerr quasinormal modes, separation constants, and spherical-spheroidal mixing coefficients, J. Open Source Softw. **4**, 1683 (2019), arXiv:1908.10377 [gr-qc].
[62] J. Skilling, Nested sampling for general bayesian computation, Bayesian Anal. **1**, 833 (2006).
[63] W. Del Pozzo and J. Veitch, `raynest`: Parallel nested sampling in python, `https://pypi.org/project/raynest/1.0.0/` (2023).
[64] E. N. Dorband, E. Berti, P. Diener, E. Schnetter, and M. Tiglio, A Numerical study of the quasinormal mode excitation of Kerr black holes, Phys. Rev. D **74**, 084028 (2006), arXiv:gr-qc/0608091.
[65] L. T. London, Modeling ringdown. II. Aligned-spin binary black holes, implications for data analysis and fundamental theory, Phys. Rev. D **102**, 084052 (2020), arXiv:1801.08208 [gr-qc].
[66] R. Panosso Macedo, Hyperboloidal framework for the Kerr spacetime, Class. Quant. Grav. **37**, 065019 (2020), arXiv:1910.13452 [gr-qc].
[67] W. Krivan, P. Laguna, P. Papadopoulos, and N. Andersson, Dynamics of perturbations of rotating black holes, Phys. Rev. D **56**, 3395 (1997), arXiv:gr-qc/9702048.
[68] E. Berti and V. Cardoso, Quasinormal ringing of Kerr black holes. I. The Excitation factors, Phys. Rev. D **74**, 104020 (2006), arXiv:gr-qc/0605118.
[69] M. H.-Y. Cheung, E. Berti, V. Baibhav, and R. Cotesta, Extracting linear and nonlinear quasinormal modes from black hole merger simulations, (2023), arXiv:2310.04489 [gr-qc].
[70] F. Carrasco, L. Lehner, R. C. Myers, O. Reula, and A. Singh, Turbulent flows for relativistic conformal fluids in 2+1 dimensions, Phys. Rev. D **86**, 126006 (2012), arXiv:1210.6702 [hep-th].
[71] S. R. Green, F. Carrasco, and L. Lehner, Holographic Path to the Turbulent Side of Gravity, Phys. Rev. X **4**, 011001 (2014), arXiv:1309.7940 [hep-th].
[72] A. Adams, P. M. Chesler, and H. Liu, Holographic turbulence, Phys. Rev. Lett. **112**, 151602 (2014), arXiv:1307.7267 [hep-th].
[73] J. Redondo-Yuste and L. Lehner, Non-linear black hole dynamics and Carrollian fluids, JHEP **02**, 240, arXiv:2212.06175 [gr-qc].
[74] H. Zhu *et al.*, Nonlinear Effects In Black Hole Ringdown From Scattering Experiments I: spin and initial data dependence of quadratic mode coupling, (2024), arXiv:2401.00805 [gr-qc].
[75] S. Ma and H. Yang, The excitation of quadratic quasinormal modes for Kerr black holes, (2024), arXiv:2401.15516 [gr-qc].